

3-D Photonic Circuit Technology

Maura Raburn, Bin Liu, *Member, IEEE*, Katharina Rauscher, Yae Okuno, Nadir Dagli, *Member, IEEE*, and John E. Bowers, *Fellow, IEEE*

Invited Paper

Abstract—Vertically coupled, wafer-bonded III–V semiconductor waveguide devices provide a means to obtain more powerful, compact photonic integrated circuits and allow for the combination of different materials onto a single chip. Various switching, filtering, multiplexing, and beam splitting devices in the InP–InGaAsP and GaAs–AlGaAs systems for signals in the 1550-nm range have been realized. An investigation of optimal optical add-drop multiplexer waveguide layout shapes has been performed through integration of the coupled-mode Riccati equation, providing potential sidelobe levels of less than –32 dB and filter bandwidths over 20% narrower than those of previous devices. Effects of nonideal processing conditions on filter performance are analyzed as well.

Index Terms—Fourier transforms, Optical directional couplers, optical switches, optical waveguide theory, Riccati equations, semiconductor waveguides, wafer bonding, wavelength-division multiplexing.

I. INTRODUCTION

THE DEVELOPMENT of three-dimensional (3-D) photonic integrated circuits (PICs) is critical for the optoelectronic IC industry to match the advances witnessed by the electronic IC industry. There are many advantages to shifting from in-plane circuits to those capable of routing in three dimensions. Traditional two-dimensional (2-D) PICs are limited by substrate size and the number of electrical and optical connections that can be made to the chip. This is a problem for the increasingly dense, complicated circuits developed today. By making the leap to multilayer interconnects, more compact devices can be obtained and further creativity in circuit design is afforded. Vertical integration to avoid the crossing of physical beam paths can lead to lower crosstalk as well. Also, because different types of devices (lasers, detectors, switches, etc.) are often best made with different materials, methods of integrating different materials onto a single chip must be addressed. Finally, some devices can be made smaller when vertical integration, rather than lateral integration, is employed. Three-dimensional routing of signals will thus be very advantageous for significantly more compact and powerful photonic ICs, such as the one shown in Fig. 1.

Manuscript received April 1, 2002; revised May 28, 2002. This work was supported by Walsin Lihwa Corporation.

M. Raburn, K. Rauscher, Y. Okuno, N. Dagli, and J. E. Bowers are with the Electrical and Computer Engineering Department, University of California, Santa Barbara, CA 93106 USA.

B. Liu is with the Calient Networks, Goleta, CA 93117 USA.
Digital Object Identifier 10.1109/JSTQE.2002.801743.

Despite the need for 3-D PIC development, relatively few approaches to this goal have been published so far. Other technologies include that of bonded vertically coupled micro-ring resonators [1], [2], micro-optoelectronic mechanical systems (MOEMS) devices [3], [4], photonic crystals [5], and three-dimensionally integrated optical polymer waveguides [6].

We have chosen a direct-contact wafer bonded vertically coupled InP–InGaAsP and GaAs–AlGaAs waveguide arrangement to allow device operation over a broad range for wavelength-division-multiplexing (WDM) applications and compatibility with other material systems and devices operated around 1550 nm. This choice of materials also allows for switching through the electrooptic and carrier injection effects with reasonable losses. Our initial effort began with the development of symmetric parallel waveguide couplers with laterally separated inputs and outputs [7] that evolved to have better filtering through the use of asymmetric design [8], [9] and x-crossed waveguide layouts [10], and easier fabrication through the use of double-sided processing [11]. Four-port devices were cascaded to make devices for more than two channels [12], [13]. Push–pull configuration optical switches [14] and devices of more than two layers [15] were also fabricated.

II. OPTICAL MULTIPLEXERS

Several variations on multiplexers and optical add–drop multiplexers (OADMs) have been developed. These consist of both devices with parallel waveguides and devices with guides that form x-crossings. Couplers created in a single epitaxial growth, as well as those made by bonding between different material systems, are included.

The initial fused vertical coupler effort [7] was satisfactory for obtaining laterally separated inputs and outputs and demonstrating coupling from input to output with a coupling length of only 62 μm and waveguide loss of only 1.1 dB/cm. Improvements to the structure and material compositions were made to enable the creation of multichannel, narrower bandwidth, low-crosstalk devices. Simulations showed that slight asymmetries in the waveguide shapes and indices lead to improved extinction ratios [8]. Devices fabricated using double-sided processing were created to allow further design flexibility and reduce the number of required epitaxial growths [11]. Through a combination of several of the above approaches, multichannel wavelength multiplexers were made from cascaded 3-D vertical couplers [12]. These two-, four-, and eight-channel couplers had 17-nm channel spacings with crosstalk as low as 20 dB.

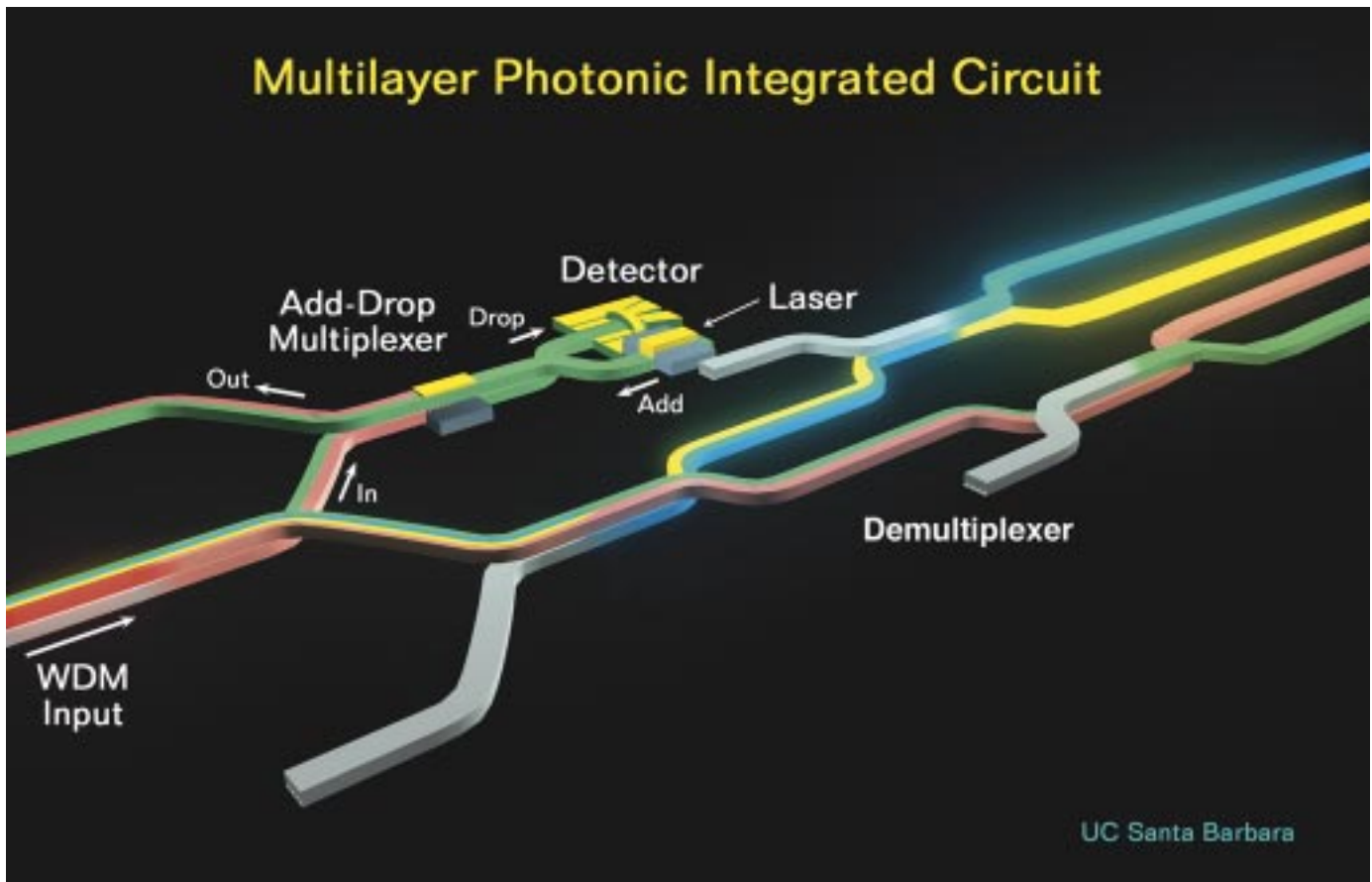


Fig. 1. Illustration of potential use of 3-D PIC technology.

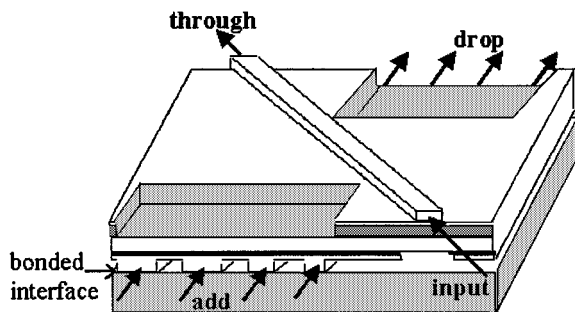


Fig. 2. Layout of the four-channel OADM.

For further improvements, it was found that alterations to the waveguide dimensions and indices as well as the waveguide layout were beneficial. Narrower filter bandwidths and a polarization sensitivity reduction by a factor of 12 were obtained through bonding InP to GaAs to create waveguides with greater waveguide dispersion differences [9]. Improved filtering is obtained because the top and bottom waveguide effective indices have different slopes as a function of wavelength and thus the indices differ greatly away from the center wavelength where they are equal. These bandwidth and polarization sensitivity improvements were adapted for the single epitaxial growth technique by using guiding InGaAsP layers of different bandgaps and thicknesses and different cladding layer thicknesses. It was also found that OADM's composed of straight,

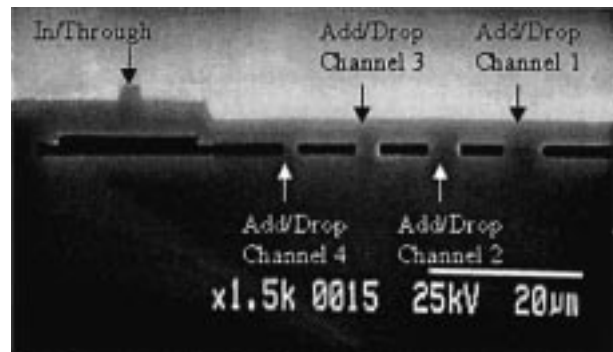


Fig. 3. SEM of cleaved facet of four-channel x-crossing OADM, including in/through waveguide and four add/drop waveguides.

x-crossed waveguides have much narrower bandwidths and sidelobes than parallel waveguide couplers [10]. The device layout is shown in Fig. 2 and an SEM of a cleaved facet is shown in Fig. 3. OADM's with sidelobe levels of -26 dB and coupling efficiencies of 97% at a central wavelength of 1560 nm were realized at a crossing angle of 0.25° . These devices had waveguide cores of $1\text{-}\mu\text{m}$ -thick $\lambda_g = 1100$ nm InGaAsP and $0.21\text{-}\mu\text{m}$ -thick 1400-nm InP to provide a sufficient waveguide dispersion difference for narrow filtering [10]. Four-channel x-crossing OADM's were then fabricated using a similar design to illustrate the potential of vertically coupled devices with no horizontally coupled counterpart of similar

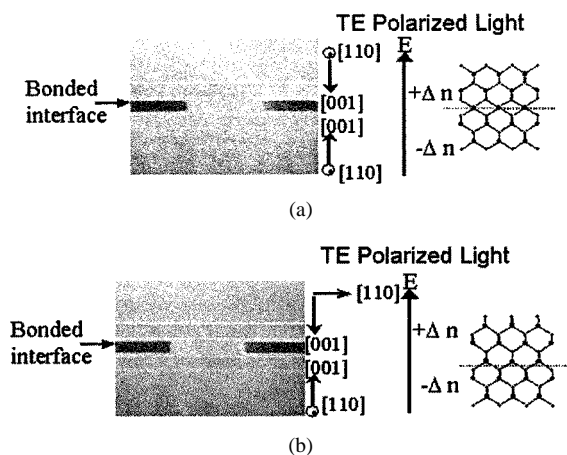


Fig. 4. SEM images and crystal orientations of cleaved antiphase and in-phase bonded vertical coupler switches. (a) Antiphase bonded vertical coupler: crystal symmetry has been inverted macroscopically. (b) In-phase bonded vertical coupler: Crystal symmetry is the same as grown material.

characteristics [13]. Work is currently underway to realize a shorter, narrower-bandwidth OADM tunable through refractive index modulation via the carrier injection effect.

III. OTHER DEVICES

Other devices include optical switches and devices of more than two bonded layers. Initially, an InP–InGaAsP vertical coupler switch that required a 12-V reverse bias for a 6.9-mm-long device was fabricated [16]. It was shown that switching at 12 V reverse bias for a 6.9-mm-long device could be achieved with a single electrode only when the crystal symmetry was inverted during fusion to achieve a push–pull configuration [14]. The cleaved facets and crystal orientations of the two configurations are shown in Fig. 4. The measurement results are shown in Fig. 5. The anisotropic linear electrooptic effect was applied in the InP–InGaAsP zinc-blend crystal to allow index changes of opposite sign in the two waveguides with different crystal symmetries. No switching was observed with the identical structure for which the two guiding layers were bonded to have the same crystal symmetry.

Also noteworthy is a three-layer double-bonded InP–InGaAsP 1:8 beam splitter formed from cascaded vertical couplers, shown in Fig. 6 [15]. The strongly coupled waveguides allowed a 583- μm device length, most of which consisted of *s*-bends for lateral waveguide separation by 15 μm . The splitter is hundreds of times shorter than the equivalent horizontal coupler. It illustrated the use of multiple vertical-layer optical interconnects for 3-D routing of optical signals. This multilayer device could be transformed into a demultiplexer through a slight change to the lengths of the coupling regions, utilizing the wavelength dependence of the coupling.

IV. ANALYSIS TECHNIQUES

Several analysis techniques are used to design the vertically coupled waveguide structures. First, the transfer matrix method (TMM) [17] is used perpendicular to the substrate surface to calculate the effective index of various 1-D multilayer slab waveguides. The one-dimensional (1-D) effective index method (EIM)

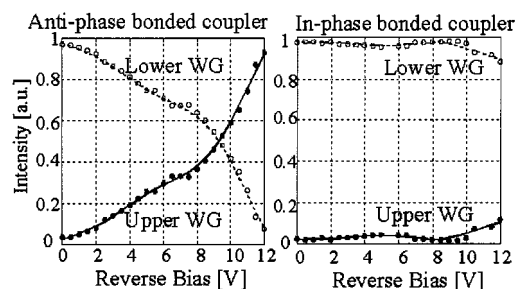


Fig. 5. The light intensity at the output of upper (solid line) and lower (dashed line) waveguides of antiphase and in-phase fused vertical coupler push–pull switch as a function of reverse bias voltage.

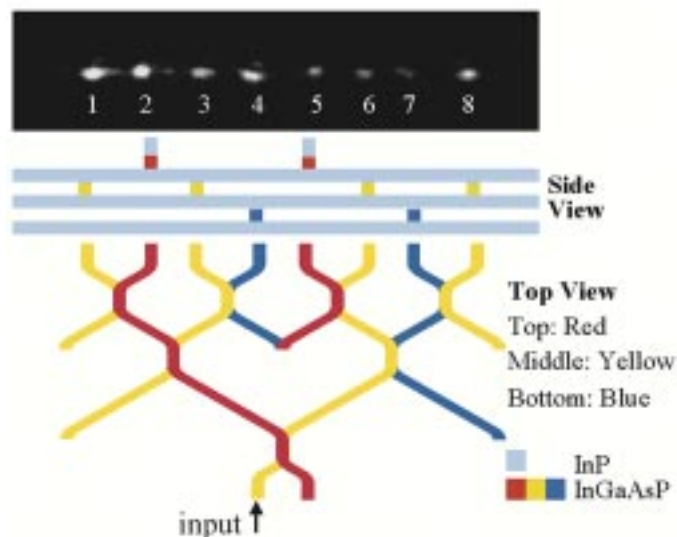


Fig. 6. Three-layer beam splitter output at $\lambda = 1483$ nm as captured by IR camera, and corresponding waveguide layout. The beam splitter is composed of InP and $\lambda_g = 1300$ nm InGaAsP.

[18] can then be used parallel to the substrate surface using the TMM results to calculate the effective index of the complete 2-D waveguide profile. These methods are used to preliminarily design the top and bottom waveguide widths, layer heights, and layer indices such that their effective indices match at a desired wavelength.

Device operation is based on coherent coupling of light between the top and bottom waveguides through two-mode interference. That is, the coupling of light is due to the overlap of the evanescent fields of the two waveguides. If the difference between the effective indices of two waveguides in close proximity over a long range is very small, light entering one waveguide will couple completely to the other guide after a given length. Thinner waveguides of lower core refractive index, by providing less modal confinement, will increase the overlap integral of the two modes of adjacent waveguides. Decreasing the thickness of the separation layer between the cores will give stronger coupling as well. For filtering devices, dissimilar indices for the top and bottom waveguides are chosen because the difference in the material and waveguide dispersion allows complete coupling over a much narrower wavelength range than with identical coupled waveguides. Away from the center wavelength, the coupling will become very small due to a phase mismatch. Filtering devices are also chosen to couple light multiple

times from input to drop waveguide over the device length for narrower bandwidths as well.

The finite-difference method (FDM) [18] is used to determine the waveguide mode profile. By performing the modal overlap integral, the coupling coefficient for different waveguide spacings can be found. Coupled-mode theory can then be used to calculate the power transfer between waveguides as a function of device length for varied coupler shapes. Finally, the beam propagation method (BPM) [19] is implemented with commercial software to check the results of the above calculations.

V. WAVEGUIDE TAPER FUNCTIONS

The optimal design of device mask layout includes the reduction of sidelobe levels. Parallel waveguides have prohibitively high sidelobes that often prevent them from being used as effective filters. Substantial improvement in the drop port sidelobe levels are observed with the transition from parallel to crossed x-shaped waveguides. Further improvement is possible, and this section analyzes the theoretical approach. Let R and S be defined as the complex amplitudes of the incident and coupled waves in the device. The relationship between R and S for codirectional coupling takes the form of a single nonlinear Riccati equation where S and R are expressed in terms of a variable ρ (defined as their ratio multiplied by a phase factor) [20], [21]:

$$\frac{d\rho}{dz} = -j \left(2\delta + \frac{d\phi}{dz} \right) \rho + j\kappa(\rho^2 - 1) \quad (1)$$

where

$$\rho = \frac{S}{R} e^{-j\phi}. \quad (2)$$

Here, κ is the coupling coefficient, ϕ is a measure of the spatial variation in the phase matching condition, and z is the coordinate in the propagation direction. δ is a measure of the deviation of the wavelength of operation from the center wavelength for which the device was designed to couple 100%:

$$\delta = \frac{2\pi}{\lambda} (n_{\text{eff}1} - n_{\text{eff}2}) \quad (3)$$

where $n_{\text{eff}1/2}$ is the effective index of the top/bottom waveguide. The coupled-mode equation (1) can be numerically integrated over the device length to find ρ at the device output. A fourth-order Runge–Kutta integration is used because of accuracy and ease of implementation.

When little power is coupled ($\rho \ll 1$), the solution of the above Riccati equation becomes much simpler. For this case, a Fourier transform relation exists between ρ and the coupling coefficient κ [21]:

$$\rho \left(\frac{L}{2} \right) = -j e^{-j(\phi + \delta L)} \int_{-\frac{L}{2}}^{\frac{L}{2}} \kappa(z) e^{j(2\delta z + \phi)} dz \quad (4)$$

where L is defined as the device length. Fourier transform simulations were performed to corroborate the Riccati equation numerical integration solution for low coupled powers.

Using either of the two approaches, the filter response in terms of the fraction of input power coupled to the drop port can be found by noting that

$$\frac{P_{\text{coupled}}}{P_{\text{input}}} = \frac{|S|^2}{|S|^2 + |R|^2} = \frac{|\rho^2|}{|\rho^2| + 1}. \quad (5)$$

Thus, we have two methods to relate coupled power to coupling coefficient κ : integration of (1) or evaluation of (4).

To find the bandwidth, sidelobes, and passband shape for coupling corresponding to any arbitrary function, we set $\kappa(z)$ equal to the function multiplied by a factor dependent on the number of times coupling back and forth over the length (three for these simulations), the device length L , and a normalization term. One can then determine the passband shape in the frequency domain of a device with this $\kappa(z)$ by calculating the coupled power using (1) or (4) over the wavelength deviation (δ) range of interest. κ can be calculated for a particular waveguide spacing using the finite difference technique to determine the mode profiles of the top and bottom waveguides and integrating over the dot product of the profiles [18]. In this manner, κ can be found for any waveguide spacing and hence the waveguide layout and device length for any $\kappa(z)$ can be determined.

Many functions from filter theory [22] were compared in terms of bandwidth, sidelobe level, and length using both the fourth order Runge–Kutta integration and Fourier transform analysis. The results are shown in Fig. 7. All devices except the parallel waveguides were designed to completely couple light back and forth three times between the input and drop waveguides, with at least $10\text{-}\mu\text{m}$ separation between guides at the device edges. $10\text{ }\mu\text{m}$ was found to be a sufficient separation between guides to reduce the coupling to zero. The parallel waveguides were simulated to have no lateral separation. These conditions were used instead of a requirement that the devices be the same length because otherwise many devices would be much longer than necessary. It is worth noting that sidelobe levels of less than -32 dB and filter bandwidths over 20% narrower than those of the previous x-crossing devices are possible with certain coupler shapes. An illustration of the spatial layouts of couplers with $\kappa(z)$ proportional to a few of these functions is provided in Fig. 8.

The device simulations for which $\kappa(z)$ is set proportional to Gaussian, adjusted Hamming, and modified Blackman functions were judged to be the best based on sidelobe levels, filter bandwidths, and device length. Gaussian and modified Blackman had the lowest sidelobes of all functions simulated, less than -30 dB . Adjusted Hamming is hundreds of microns shorter than most of the other devices with reasonable bandwidths and sidelobes. A comparison of the filter performance of these three functions is shown in Fig. 9. Experimental efforts to fabricate and test the Gaussian, Adjusted Hamming, and Modified Blackman tapers are presently underway.

A comparison of the filter performance for the fourth-order Runge–Kutta integration, Fourier transform, and BPM [19] are shown in Fig. 10. The three approaches show reasonable agreement for small deviations from the center wavelength. The fast, and easy-to-compute Fourier transform relation is thus considered to work well to obtain a quick approximation for small δ . The BPM and the Runge–Kutta integration approaches are both considered “actual” solutions. The difference between the two “actual” solutions is due to time and memory limitations of grid spacings and step sizes in the computations. The BPM involves a huge number of calculations as the light is simulated to traverse the device step by step with very small step size. Thus, for small coupled powers, a very large number of significant figures

Name	Taper Function	-20dB half width	peak first min	side-lobe	Length
Modified Blackman	$1+1.125\cos(2\pi z/L)+0.183\cos(4\pi z/L)$	7.5nm	9.1nm	-32.4dB	4001 μm
Adjusted Hamming	$1+0.93\cos(2\pi z/L)$	6.5nm	7.5nm	-22.3dB	3718 μm
Gaussian	$\exp(-\pi 4.25 z^2/L^2)$	6.3nm	7.6nm	-31.5dB	4011 μm
X, $\theta=0.3^\circ$	Straight crossing wgs	7.4nm	8.5nm	-26dB	4000 μm
Kaiser $\gamma=10$	$\frac{\gamma}{\sinh(\gamma)} I_0 \left[\gamma \sqrt{1 - \left(\frac{2z}{L}\right)^2} \right]$	8.5nm	9.6nm	-27.2dB	3793 μm
Raised Cos	$1 + \cos(2\pi z/L)$	9.1nm	6.5nm	-18.7dB	4277 μm
Hamming	$1 + 0.852\cos(2\pi z/L)$	5.9nm	6.8nm	-24.9dB	3960 μm
Blackman	$1+1.19\cos(2\pi z/L)+0.19\cos(4\pi z/L)$	7.5nm	8.5nm	-23.3dB	4000 μm
Butterworth N=3 $z_c=0.185L$	$\frac{1}{\sqrt{1 + \left(\frac{z}{z_c}\right)^{2N}}}$	11.5nm	12.5nm	-23.9dB	3904 μm
Chebyshev N=3, $\epsilon=2$, $z_c=0.17L$	$\frac{1}{1 + \epsilon^2 \left(\cos \left(N \arccos \left(\frac{z}{z_c} \right) \right) \right)^2}$	18.6nm	12.3nm	-14.2dB	3492 μm
Parallel wg	1	92.9nm	9.2nm	-4.4dB	1927 μm
Windowed Sinc, $b=3/L$	$\frac{\sin(2bz)}{z} (1+0.93\cos(2\pi z/L))$	8.1nm	9.3nm	-26.3dB	3653 μm
Sinc, $b=3/L$	$\frac{\sin(2bz)}{z}$	11.4nm	7.1nm	-14.4dB	3126 μm

Fig. 7. -20-dB half width, first minima of central peak, and magnitude of first sidelobe for various taper functions using fourth-order Runge-Kutta numerical integration of coupled-mode Ricatti equation. L denotes device length.

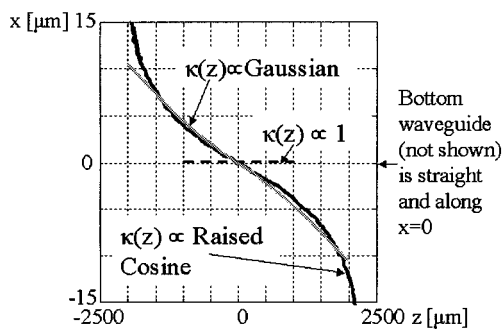


Fig. 8. Illustration of waveguide layouts as they would actually appear on mask for devices for which $\kappa(z) \propto$ Gaussian, Raised Cosine, and 1.

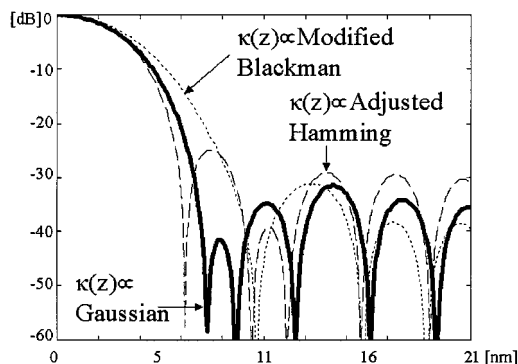


Fig. 9. Comparison of coupled power vs. wavelength for Gaussian, adjusted Hamming, and modified Blackman functions using fourth-order Runge-Kutta numerical integration of the Ricatti equation.

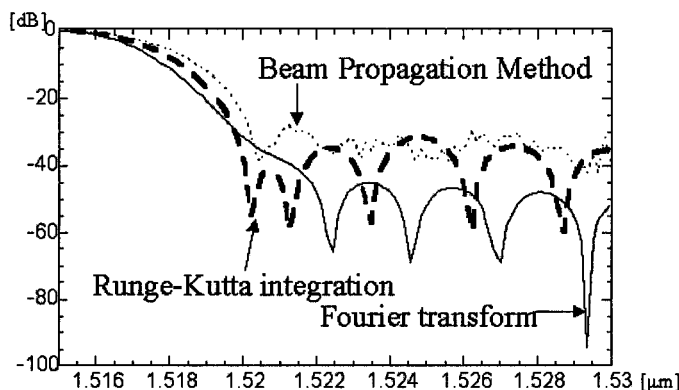


Fig. 10. Comparison of OADM performance (coupled power vs. wavelength) for coupler for which $\kappa(z) \propto$ Gaussian with fourth-order Runge-Kutta numerical integration of the Ricatti equation, Fourier transform, and beam propagation method analyses.

must be retained to avoid round-off errors. This is why the BPM curve is not smooth for large wavelength deviations where coupling is low.

VI. NONIDEAL PROCESSING CONDITIONS

One new concern for vertically coupled waveguide devices is waveguide alignment. Traditional horizontally coupled devices are more sensitive to waveguide spacings but also typically require only one mask layer for patterning the guides so alignment

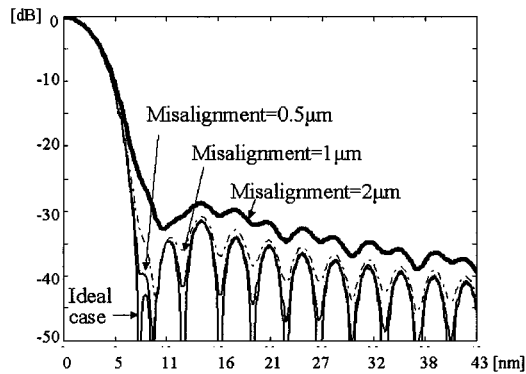


Fig. 11. Coupled power versus wavelength for coupler for which $\kappa(z) \propto$ Gaussian when laterally misaligned by 0.5, 1, and 2 μm . The waveguides are 3 μm wide and composed of a structure similar to that of Fig. 4.

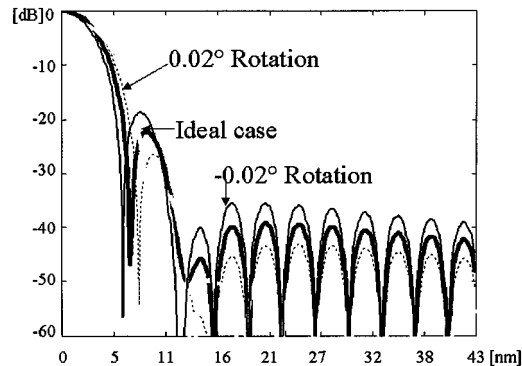


Fig. 12. Coupled power versus wavelength for coupler for which $\kappa(z) \propto$ Altered Hamming when misaligned through a rotation about the center of 0.02, and -0.02 . The waveguides are 3 μm wide and composed of a structure similar to that of Fig. 4.

has not been an issue. Little has been reported regarding such recent alignment issues [23].

The Gaussian and adjusted Hamming waveguide layouts from above were used in the simulations because they had the most desirable filter characteristics overall. Vertical misalignment is not a concern because one of the two waveguides is assumed to be straight. However, lateral misalignment can lead to filter degradation and can be particularly problematic when aligning a “top” mask layer to layers hidden below the surface after bonding and substrate removal.

To determine the effects of lateral misalignment, the spatial waveguide layout was first determined for a Gaussian $\kappa(z)$. Then, an offset was added to the lateral coordinate of the waveguide layout to “misalign” the guide. $\kappa'(z)$ of this new layout was then calculated. The filter response for lateral misalignment, shown in Fig. 11, was found by integrating the Riccati coupling equation using the new $\kappa'(z)$. Though a misalignment by 2 μm is rather extreme, it is included to illustrate the degree of misalignment tolerated by vertically coupled waveguide devices. Thus, we note that device performance is not greatly compromised by misalignments on the order of 1 μm or less.

Of course, misalignment is not limited to vertical and lateral positional offsets of the entire mask layer. Rotational misalign-

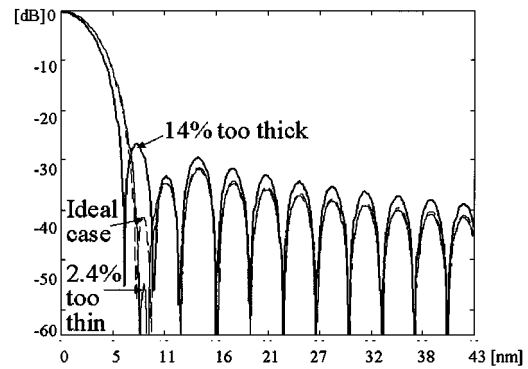


Fig. 13. Coupled power versus wavelength for coupler for which $\kappa(z) \propto$ Gaussian when the thinner, higher index guiding layer is grown to the wrong thickness. The waveguides are 3 μm wide.

ment can be a problem when align marks are not sufficiently far apart. Calculation of rotational misalignment is similar to that of lateral misalignment except that instead of simply adding a constant offset to the spatial waveguide layout to determine $\kappa'(z)$, the entire layout is rotated through a coordinate transformation. The results of the rotational misalignment simulation are shown in Fig. 12. In this case a range from -0.02 to $+0.02$ degree is considered. The maximum lateral misalignment of 1 μm for the device sizes we typically work with creates a rotational misalignment within this range.

Through backside illumination, misalignments of less than 0.5 μm can be obtained with IR photolithography. However, it can be difficult to measure the misalignment of the “top” and “bottom” mask layers with this technique after the patterning is completed. A more precise alignment method consists of etching alignment marks through most of the epitaxial layers before bonding such that the marks are visible on the other side of the epitaxial layer after bonding and substrate removal [23]. In this way, verniers to measure misalignment can be included so that the actual effects of the misalignment can be simulated [24].

Another potential obstacle to realizing a device as designed is imperfect epitaxial layer growth. Operating wavelengths and filter bandwidths can change significantly if layers are grown of the wrong thickness or composition. It is useful to simulate from the parameters of a nonideal growth the required alteration to waveguide widths and heights for desired device operation in order to change them if possible before processing. Nonideal growths were simulated by calculating κ as a function of waveguide separation for the poor growth using the finite difference technique and coupled-mode theory as explained above. The waveguide separation as a function of z for an ideal growth, as would appear on the mask, was then compared to this κ to obtain $\kappa(z)$. Finally, the Riccati equation with this $\kappa(z)$ was integrated to find the filter behavior for poor growth. Results are shown for a guiding layer grown too thick and too thin in Fig. 13. The thickness range indicated in this figure covers the range we encountered in our work so far. One can see that sidelobe levels may increase greatly with only a small difference in waveguide thickness. Devices made from material of undesirable composition can be simulated in a similar manner.

For accuracy and speed, the fourth-order Runge–Kutta integration of the Riccati coupled mode equation was used for all misalignment and nonideal growth simulations.

VII. CONCLUSION

Much progress in the field of 3-D photonic circuits has been achieved in recent years. Ultrashort vertical couplers can be made with 100% coupling in 60 μm . Push–pull switches utilizing a bonded crystal inversion have been made. Three-layer 1:8 splitters have been demonstrated. The effect of the spatial dependence of coupling on filter shape is analyzed. The sensitivity of the design to processing and growth imperfections is analyzed. These results apply to bonded structures as well as other vertically coupled structures. OADM filter sidelobe levels have been reduced to -26 dB experimentally. Sidelobe levels less than -32 dB have been simulated by tailoring the waveguide shapes. Experimental testing is underway. Through combining these various approaches, electronically tuned WDM devices of low bandwidth and sidelobe levels composed of different materials will be possible.

REFERENCES

- [1] R. Grover, P. P. Absil, V. Van, J. V. Hryniewicz, B. E. Little, O. King, L. C. Calhoun, F. G. Johnson, and P.-T. Ho, "Vertically coupled GaInAsP-InP microring resonators," *Opt. Lett.*, vol. 26, no. 8, pp. 506–508, Apr. 15, 2001.
- [2] D. V. Tishinin, P. D. Dapkus, A. E. Bond, I. Kim, C. K. Lin, and J. O'Brien, "Vertical resonant couplers with precise coupling efficiency control fabricated by wafer bonding," *IEEE Photon. Technol. Lett.*, vol. 11, pp. 1003–1005, Aug. 1999.
- [3] M. Wu, "Micromachining for optical and optoelectronic systems," *Proc. IEEE*, vol. 85, pp. 1833–1856, Nov. 1997.
- [4] V. A. Aksyuk *et al.*, "Lucent microstar micromirror array technology for large optical crossconnects," *Proc. SPIE*, vol. 4178, pp. 320–324, 2000.
- [5] A. Chutinan, M. Mochizuki, M. Imada, and S. Noda, "Surface-emitting channel drop filters using single defects in two-dimensional photonic crystal slabs," *Appl. Phys. Lett.*, vol. 79, no. 17, pp. 2690–2692, Oct. 22, 2001.
- [6] S. M. Garner, S.-S. Lee, V. Chuyanov, A. Chen, A. Yacoubian, W. H. Steier, and L. R. Dalton, "Three-dimensional integrated optics using polymers," *IEEE J. Quantum Electron.*, vol. 35, pp. 1146–1155, Aug. 1999.
- [7] B. Liu, A. Shakouri, P. Abraham, B. G. Kim, A. W. Jackson, and J. E. Bowers, "Fused vertical couplers," *Appl. Phys. Lett.*, vol. 72, no. 21, pp. 2637–2638, May 1998.
- [8] B. G. Kim, A. Shakouri, B. Liu, and J. E. Bowers, "Improved extinction ratio in ultra short directional couplers using asymmetric structures," *Jpn. J. Appl. Phys.*, vol. 37, no. 8A, pp. L930–L932, Aug. 1998.
- [9] B. Liu, A. Shakouri, P. Abraham, Y. J. Chiu, and J. E. Bowers, "Fused III–V vertical coupler filter with reduced polarization sensitivity," *Electron. Lett.*, vol. 35, no. 6, pp. 1–2, Mar. 1999.
- [10] B. Liu, A. Shakouri, P. Abraham, and J. E. Bowers, "Optical add/drop multiplexers based on X-crossing vertical coupler filters," *IEEE Photon. Technol. Lett.*, vol. 12, pp. 410–412, Apr. 2000.
- [11] —, "Vertical coupler with separated inputs and outputs fabricated using double-sided process," *Electron. Lett.*, vol. 35, no. 18, pp. 1552–1554, Sept. 1999.
- [12] —, "A wavelength multiplexer using cascaded three-dimensional vertical couplers," *Appl. Phys. Lett.*, vol. 76, no. 3, pp. 282–284, Jan. 2000.
- [13] M. Raburn, B. Liu, Y. Okuno, and J. E. Bowers, "InP-InGaAsP wafer-bonded vertically coupled X-crossing multiple channel optical add-drop multiplexer," *IEEE Photon. Technol. Lett.*, vol. 13, pp. 579–581, June 2001.
- [14] B. Liu, A. Shakouri, P. Abraham, and J. E. Bowers, "Push-pull fused vertical coupler switch," *IEEE Photon. Technol. Lett.*, vol. 11, pp. 662–664, June 1999.

- [15] M. Raburn, B. Liu, P. Abraham, and J. E. Bowers, "Double-bonded InP-InGaAsP vertical coupler 1:8 beam splitter," *IEEE Photon. Technol. Lett.*, vol. 12, pp. 1639–1641, Dec. 2000.
- [16] B. Liu, A. Shakouri, P. Abraham, and J. E. Bowers, "Fused vertical coupler switches," *Electron. Lett.*, vol. 34, no. 22, pp. 2160–2061, Sept. 1998.
- [17] J. Chilwell and I. Hodgkinson, "Thin-films field-transfer matrix theory of planar multilayer waveguides and reflection from prism-loaded waveguides," *J. Opt. Soc. Amer. A (Optics and Image Science)*, vol. 1, no. 7, pp. 742–753, July 1984.
- [18] L. A. Coldren and S. W. Corzine, *Diode Lasers and Photonic Integrated Circuits*. New York: Wiley, 1995, ch. 7, app. 3, 16.
- [19] BeamProp, Version 3.0, Rsoft, Inc., 1999.
- [20] R. C. Alferness and P. S. Cross, "Filter characteristics of codirectionally coupled waveguides with weighted coupling," *IEEE J. Quantum Electron.*, vol. QE-14, pp. 843–847, Nov. 1978.
- [21] H. Kogelnik, "Filter response of nonuniform almost-periodic structures," *Bell. Syst. Tech. J.*, vol. 55, pp. 109–126, 1976.
- [22] A. Kar-Roy and C. S. Tsai, "Ultralow sidelobe-level integrated acousto-optic tunable filters using tapered-gap surface acoustic wave directional couplers," *J. Lightwave Technol.*, vol. 12, pp. 977–982, June 1994.
- [23] P. P. Absil, J. V. Hryniewicz, B. E. Little, F. G. Johnson, K. J. Ritter, and P.-T. Ho, "Vertically coupled microring resonators using polymer wafer bonding," *IEEE Photon. Technol. Lett.*, vol. 13, pp. 49–51, Jan. 2001.
- [24] R. Grover, private communication.



Maura Raburn received the B.S. degree in applied physics from California Institute of Technology, Pasadena, in 1998, and the M.S. degree in electrical engineering from the University of California at Santa Barbara (UCSB) in 2000. She is working toward her Ph.D. degree at UCSB.

Her interests include wafer bonding, the fabrication and design of vertically coupled waveguide devices and three-dimensional integrated circuits, and the related physics.



Bin Liu (S'99–M'00) received the B.S. degree from Zhejiang University, China, in 1990, the M.S. degree from Shanghai Institute of Optics and Fine Mechanics, Chinese Academy of Sciences in 1995, and the Ph.D. degree at the University of California, Santa Barbara in 2000.

Since 2000, he is with Calient Networks, Santa Barbara, CA. He is working on the fabrication of MEMS-based optical switching and microoptics.



Katharina Rauscher is working toward the Diploma in electrical engineering from the University in Stuttgart, Germany.

She is a visiting researcher at the University of California at Santa Barbara (UCSB), where she joined the group in May 2001. While at UCSB, she is working on her Diploma project, which involves research on vertically coupled waveguide devices.



Yae Okuno received the B.S. degree in nuclear engineering from Kyoto University, Japan, in 1990, and the M.S. degree in electrical engineering from the University of California at Berkeley in 1999.

From 1990 to 1997, she was at Hitachi Central Research Laboratory, Japan, where she worked on MOVPE of InP and GaAs, long-wavelength lasers, and wafer fusion. Joining UCSB in 1999, her research interests are wafer-fused VCSELs and MOVPE of InP and related materials.



Nadir Dagli (S'77-M'87) received the B.S. and M.S. degrees in electrical engineering from Middle East Technical University, Ankara, Turkey in 1976 and 1979, respectively, and Ph.D. degree, also in electrical engineering, from Massachusetts Institute of Technology, Cambridge, MA in 1986. During his Ph.D. research, he worked on the design, fabrication and modeling of guided wave integrated optical components in III-V compound semiconductors. He also worked on III-V materials preparation by LPE and the modeling and analysis of heterojunction

bipolar transistor for microwave and millimeter-wave applications.

After graduation, he joined the Electrical and Computer Engineering Department at University of California at Santa Barbara, where he is currently a Professor. His current interests are design, fabrication and modeling of guided-wave components for optical integrated circuits, ultrafast electrooptic modulators and WDM components, calculations on the optical properties of quantum wires, and experimental study of novel quantum devices based on ballistic transport in quantum wires. He served on many different program committees and participated on a wide range of professional activities. Presently, he is serving on the Microwave Photonics Committee of IEEE Lasers and Electro Optics Society Annual Meeting, International Topical Meeting on Microwave Photonics and is the Editor-in-Chief of IEEE PHOTONICS TECHNOLOGY LETTERS.



John E. Bowers (S'78-M'81-SM'85-F'93) received the M.S. and Ph.D. degrees in applied physics from Stanford University, Stanford, CA.

He is Director of the Multidisciplinary Optical Switching Technology Center (MOST), and a Professor in the Electrical Engineering Department at the University of California, Santa Barbara. He is co-founder and a Board member of CEEM (the Center for Entrepreneurship and Engineering Management) and a member of CHIPS (Chips with Heterogeneously Integrated Photonics). He worked

for AT&T Bell Laboratories and Honeywell before joining UCSB. His research interests are primarily concerned with high frequency optoelectronic devices and physics.